

On the analysis of photo-electron spectra

C.-Z. Gao^{a,b,*}, P. M. Dinh^{a,b}, P.-G. Reinhard^c, E. Suraud^{a,b}

^a*Université de Toulouse, UPS; Laboratoire de Physique Théorique (IRSAMC),
F-31062 Toulouse Cedex, France*

^b*CNRS; LPT (IRSAMC), Université de Toulouse, F-31062 Toulouse Cedex,
France*

^c*Institut für Theoretische Physik, Universität Erlangen, D-91058 Erlangen,
Germany*

Abstract

We analyze Photo-Electron Spectra (PES) for a variety of excitation mechanisms from a simple mono-frequency laser pulse to involved combination of pulses as used, e.g., in attosecond experiments. In the case of simple pulses, the peaks in PES reflect the occupied single-particle levels in combination with the given laser frequency. This usual, simple rule may badly fail in the case of excitation pulses with mixed frequencies and if resonant modes of the system are significantly excited. We thus develop an extension of the usual rule to cover all possible excitation scenarios, including mixed frequencies in the attosecond regime. We find that the spectral distributions of dipole, monopole and quadrupole power for the given excitation taken together and properly shifted by the single-particle energies provide a pertinent picture of the PES in all situations. This leads to the derivation of a generalized relation allowing to understand photo-electron yields even in complex experimental setups.

Key words: photo-electron spectra, photo-absorption spectra

PACS: 32.80.Fb, 33.20.Xx

1 Introduction

Photo-Electron Spectroscopy (PES) has grown over decades to one of the major tools of analysis of the structure and dynamics of atoms, molecules or solids

* Corresponding author

Email-address : gao@irsamc.ups-tlse.fr

[1,2,3]. With the increasing availability and versatility of light sources, studies of PES are now found in all areas of molecular physics, in atoms and simple molecules [4] as well as in more complex systems such as clusters [5] or organic molecules [6]. The archetypal case is that a system is subject to a laser field with moderate intensity and sufficiently high frequency, such that all valence electron states can be ionized in one stroke. In this one-photon regime, the PES delivers a printout of the sequence of single particle (s.p.) energies from the occupied states [7,8]. But PES do also allow to access dynamical features. A typical example is the multiphoton regime in which ionization proceeds via absorption of several photons which is often achieved by IR photons at moderate intensity. The PES then exhibits the pattern of Multiphoton Ionization (MPI) [3,9,10] showing successive copies of the s.p. spectrum. Further increasing laser intensity leads to increasingly complex patterns, i.e., above threshold ionization (ATI) [11,12] and strong-field ionization [13,14,15].

Simple laser setups are characterized by *one* well defined photon frequency ω_{las} . The energies $E_{i,\nu}$ of the PES peaks from such sources follow a well known rule relating them to s.p. energies ε_i [9] as

$$E_{i,\nu} = \varepsilon_i + \nu\hbar\omega_{\text{las}} \quad , \quad (1)$$

where i stands for the s.p. state from which the electron is emitted and ν is the number of absorbed photons for ionization ($\nu > 1$ for MPI). In other words, the PES yield $\mathcal{Y}(E_{\text{kin}})$ is then interpreted as a sum of Dirac distributions :

$$\mathcal{Y}(E_{\text{kin}}) \leftrightarrow \sum_{\nu} \sum_i \delta(E_{\text{kin}} - E_{i,\nu}) \quad . \quad (2)$$

For high laser intensity, relation (1) has to be complemented by the energy of the ponderomotive potential U_p which represents the average kinetic energy of a free electron in the laser field [10,16]. For the sake of simplicity, we shall confine our discussion in the following to cases in which U_p remains negligible.

With the advent of a large variety of coherent light sources [17,18,19], it has become possible to access more complex dynamical scenarios, involving several frequencies and/or pulse combinations, for example, in pump-and-probe setups [20]. The latter ones even provide a time-resolved access to dynamics, at ionic pace with femtosecond (fs) [21,22] down to electronic pace with attosecond (as) pulses [23,24,25,26,27]. The PES of course remains a highly valuable tool of investigation of the dynamics, as it basically provides insight into electronic dynamics via ionization characteristics. But the simple rule Eq. (1) takes a more complicated expression in the case of a complex light pulse. For instance, in a pump-and-probe experiment where there are possibly two laser colors, one should add to the s.p. energies linear combinations of the two laser frequencies to obtain the positions of the PES peaks. This is all the more involved when it is in the multi-photon regime for which the

number of combinations grows fast. In this case, the identification of the PES peaks to a certain combination of laser frequencies can become tricky. It is thus important to understand how the PES builds up in the course of irradiation processes involving complicated laser pulses. The question is in fact even more general. There also exist experiments measuring kinetic energies of the electrons emitted after irradiation by a charged projectile [28,29] and a first theoretical exploration was proposed in [30]. This also provides a PES but now with a “photon” of mixed frequencies, as the effect of a charged projectile is basically to deliver a short electromagnetic pulse which covers a broad band of frequencies. Indeed, the shorter the pulse, the broader the band of accessible frequencies. For the sake of simplicity, we continue to call PES such kinetic electron spectra from ultra-short pulses, even if the notion of a “photon” is rather untypical here. The analysis of the PES obtained in such fast collisions can also reveal structures which can be attributed to eigenfrequencies of the system, e.g., the Mie plasmon frequency in the case of metal clusters [31,32] or C_{60} [33]. It should also be noted that the intense plasmon of metal clusters also shows up in laser-driven PES and can be spotted when scanning laser frequency around the plasmon frequency, as was outlined some years ago [34].

All in all, the PES thus reflects the typical frequencies present in the system, either those delivered from outside by a laser field or intrinsic ones as mostly visible in the case of a fast collision. It is the goal of this paper to investigate in detail this interplay of frequencies. We shall consider various types of excitations in order to scan a variety of dynamical scenarios. At the side of test systems, we perform the quantitative analysis mostly for a simple case, that is the He atom, to maintain clear signatures. The paper is organized as follows. Section 2 briefly presents the theoretical framework. Then we analyze a few typical cases involving various laser setups including state-of-the-art attotrans in Section 3. Once identified the limitations of the simple rule Eq. (1), we propose an alternative, more general, rule to cover any dynamical scenario in Section 4. Conclusions and perspectives are finally drawn in Section 5.

2 A brief sketch of theory

2.1 Basics

Our computations are done with Density Functional Theory (DFT). We work here in real-time Time-Dependent DFT at the level of the Kohn-Sham (KS) picture [35]. The system is then described by a set of single particle wave functions $\varphi_i(\mathbf{r}, t)$ which follow the time-dependent Kohn-Sham (TDKS) equations

[36]

$$i \frac{\partial \varphi_i(\mathbf{r}, t)}{\partial t} = \left[-\nabla^2 + V_{\text{eff}}(\mathbf{r}) \right] \varphi_i(\mathbf{r}, t). \quad (3)$$

We use Rydberg atomic units ($\hbar = e = 2m_e = 1$) throughout the paper except where specifically stated differently. The term V_{eff} in Eq. (3) is the KS effective potential. It is composed of three parts $V_{\text{eff}} = V_{\text{ion}} + V_{\text{H}} + V_{\text{xc}}[\rho]$. The term V_{ion} is the ionic background potential which is described by a pseudopotential, a simple local one for sodium [37] and a Goedecker-type one for helium [38]. The term V_{H} is the Hartree contribution and the last term V_{xc} represents the exchange correlation potential. The latter term is a functional of the local density $\rho(\mathbf{r}, t) = \sum_i |\varphi_i(\mathbf{r}, t)|^2$ and we work here within the time-dependent version of the Local Density Approximation (TDLDA) with the parametrization of Perdew and Wang [39]. The TDLDA is complemented by an efficient self-interaction correction term [40] which allows us to properly describe the ionization threshold [41,42].

2.2 Excitation mechanisms

In this paper, we will use various irradiation processes for the excitation : a fast colliding charged projectile, a single laser pulse, a sum of attosecond pulses, and finally an involved superposition of IR femtosecond pulse with UV attosecond pulses.

The first type of excitation is an instantaneous dipole boost of all electronic wave functions at $t = 0$, mimicking the collision with a swift ion, that is, $\varphi_i(\mathbf{r}, t = 0) = e^{i\eta \hat{D}} \varphi_i^{(0)}(\mathbf{r})$, where \hat{D} is the dipole operator, η is the boost momentum and $\varphi_i^{(0)}$ is the ground state Kohn-Sham wave function for state i .

The single laser pulse is modeled as

$$E_{\text{las}}(t) = E_0 f_T(t) \sin(\omega_{\text{las}} t), \quad (4a)$$

$$f_T(t) = \cos^2 \left(\frac{t - T/2}{T} \pi \right) \theta(t) \theta(T - t), \quad (4b)$$

where θ is the Heaviside function, T the pulse duration and ω_{las} its frequency. T takes typical values of some hundreds of fs, while we will consider in this paper either an IR frequency ($\omega_{\text{las}} = \omega_{\text{IR}} = 0.115$ Ry) or a UV one ($\omega_{\text{las}} = \omega_{\text{UV}} = 1.5$ Ry in Figure 2 and 0.5 Ry in Figure 8).

As an example of a rather complex pulse, we will consider an attosecond train of UV pulses, that is, a sum of pulses similar to that defined in Eqs. (4) but with $\omega_{\text{las}} = \omega_{\text{atto}}$ in the UV range, a pulse duration T of a fraction of fs, and each UV attopulse shifted in time. In other words, the attotrain field reads :

$$E_{\text{atto}}(t) = E_0^{(\text{atto})} \sum_{\alpha=0}^{N-1} g(t) f_T(t - t_\alpha) \sin(\omega_{\text{atto}} t) , \quad (5a)$$

$$t_\alpha = \Delta\tau + \alpha T_{\text{train}} , \quad (5b)$$

$$g(t) = \exp\left(-\frac{(t - \Delta\tau - \mathcal{T})^2}{\mathcal{T}^2/(4 \ln 2)}\right) , \quad (5c)$$

$$\mathcal{T} = N T_{\text{train}}/2 . \quad (5d)$$

Some additional parameters have been introduced here, let us explain them. In most experiments [26,27,43,44,45], an IR fs pulse is used to generate high harmonics which then serve to produce the coherent attotrain, which is usually modulated by an envelop that we denoted by g in Eq. (5c). Here, we take in our simulations a Gaussian envelop as in the experiment of [27]. (But other theoretical calculations use a \cos^2 envelop instead for a comparison with another experiment [43].) One can also play on the delay between the IR pulse and the attotrain. This delay $\Delta\tau$ is thus entering the definition of the envelop g but also in the shifting times t_α in Eq. (5b). In the present work, we fix it at $\Delta\tau = 46$ fs. As for T_{train} , it corresponds to the time separation between the maxima of two successive attopulses. Finally, the number of UV pulses in the attotrain is denoted by N and is typically about 10. It is obvious that Eq. (5a) represents a considerably complicated pulse and that it will provide a critical test case for our analysis. Figure 1 summarizes the various pulses we will use, as it displays the time profile of a single IR fs pulse (top panel), see Eqs. (4), and that of an attotrain (bottom panel), see Eqs. (5).

Finally, we will consider the superposition of an IR fs pulse and a UV attotrain, as encountered in experiments [26,27,43,44,45]. This case will represent the most difficult excitation mechanism to be understood.

2.3 Numerical treatment

The TDLDA equations are implemented on a grid in coordinate space. In the present (principle) study, we consider spherical systems so that we can recur to a 2D cylindrical representation. This considerably reduces the computational expense. The ground state of the system is determined by the damped gradient method. The time propagation uses T - V splitting. To describe ionization, we use absorbing boundary conditions. For details of the numerics, see [46,47]. A warning is in order here. Experimental PES and related effects belong to electrons in the continuum. It is known that a numerical description of outgoing waves requires careful choice of grid parameters to avoid artifacts from unwanted discretization of the continuum [48]. We therefore choose here very large numerical boxes to avoid such artifacts : for the metal cluster Na_9^+ , we use $138.4 a_0$ in the longitudinal direction (=symmetry axis) and $71.2 a_0$ in the radial one (with the same mesh size of $0.8 a_0$ in both directions), and for

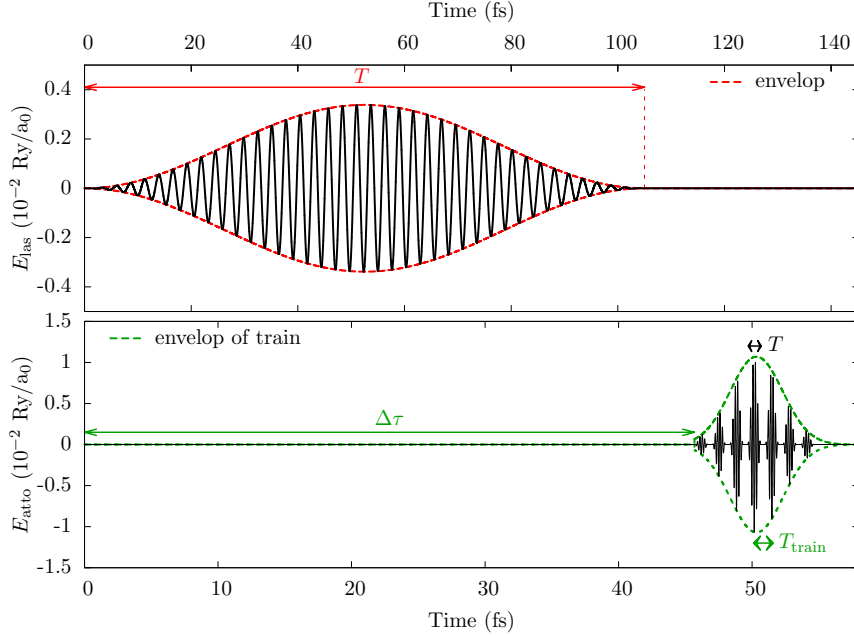


Fig. 1. Time profiles of typical laser fields considered in this paper. Top : IR femtosecond pulse as defined in Eqs. (4), with duration $T = 105$ fs, frequency $\omega_{\text{las}} = 0.115$ Ry, intensity $I = 10^{13}$ W/cm². Bottom : train of UV attosecond pulses (attotrain), as defined in Eqs. (5), with $\omega_{\text{atto}} = 1.69$ Ry, $I = 10^{12}$ W/cm², attopulse duration $T = 1$ fs, delay $\Delta\tau = 46$ fs, and attopulse separation $T_{\text{train}} = 1.33$ fs.

the He atom, we use $105.6 a_0$ and $52.8 a_0$ respectively (the mesh size being in that case $0.6 a_0$).

2.4 Observables

The spectral distribution of multipole strength is computed from TDLDA in the time domain using spectral analysis following the prescription of [49,50]. For the example of dipole strength, this proceeds as follows. Whatever the excitation mechanism (boost or finite-width laser pulse), we record the dipole moment $D(t) = \int d^3\mathbf{r} z \rho(\mathbf{r}, t)$ as it evolves over the TDLDA simulation. Note that we consider here the dipole along laser polarization axis, denoted by z , or, generally speaking, along the excitation direction and/or symmetry axis of the system. The time signal $D(t)$ is Fourier transformed into frequency domain, yielding $\tilde{D}(\omega)$. The dipole power spectrum is then $P_D(\omega) \propto |\tilde{D}(\omega)|^2$. We consider here the power spectrum rather than the usual dipole strength (which is the imaginary part of $\tilde{D}(\omega)$ [50]) since we compare it to the PES, which is also a power spectrum.

The central ingredient of the paper is the PES, the spectrum of asymptotic kinetic energies of emitted electrons. Its computation has been worked out

in detail in several papers [34,51,52,53] ; for a recent extension to the case of strong fields, see [54]. We briefly present the procedure for the sake of completeness. It is directly based on the KS s. p. wave functions [34]. We choose a “measuring point” $\mathbf{r}_{\mathcal{M}}$ located far away from the system and just before the absorbing boundaries. We record all s. p. wave functions $\varphi_i(\mathbf{r}_{\mathcal{M}}, t)$ at that point all along the simulation time. Because of the large distance from the center of the system, we can neglect the KS field and assume a free particle dynamics (strong fields, not encountered here, require to consider electron motion in the ponderomotive field of the laser [54]). In addition, because we are close to the absorbing boundary and far away from the source, only outgoing waves with momentum $\mathbf{k} = k\mathbf{r}_{\mathcal{M}}/r_{\mathcal{M}}$ will pass the point $\mathbf{r}_{\mathcal{M}}$. This allows us to establish a revertible relation $\omega \leftrightarrow k$ between momentum and energy. The PES yield $\mathcal{Y}_{\Omega_{\mathbf{r}_{\mathcal{M}}}}(E_{\text{kin}})$ can then be obtained from Fourier transformation from time t to frequency ω of the KS orbitals φ_j :

$$\mathcal{Y}_{\Omega_{\mathbf{r}_{\mathcal{M}}}}(E_{\text{kin}}) \propto \sum_{j=1}^N |\tilde{\varphi}_j(\mathbf{r}_{\mathcal{M}}, E_{\text{kin}})|^2. \quad (6)$$

The quantity $\Omega_{\mathbf{r}_{\mathcal{M}}}$ represents here the solid angle related to the direction of $\mathbf{r}_{\mathcal{M}}$, $\tilde{\varphi}_j(\mathbf{r}_{\mathcal{M}}, E_{\text{kin}})$ is the time-frequency Fourier transform of $\varphi_j(\mathbf{r}_{\mathcal{M}}, t)$ and the kinetic energy reads $E_{\text{kin}} = k^2/2 = \omega$ [54]. Performing such an analysis at a dense mesh of measuring points allows us to compute the fully energy- and angular-resolved PES [42,55]. However, since we are interested here purely in spectral features, we shall restrict the analysis to a point along the laser polarization (or symmetry) axis.

3 Typical PES interpretation and limitations thereof

3.1 A simple example

We start with illustrating Eq. (1) through a simple test case, namely the Na_9^+ cluster irradiated by a single UV laser pulse, see Eq. (4), of frequency $\omega_{\text{las}} = 1.5$ Ry, intensity $I = 10^{13}$ W/cm² and duration $T = 232$ fs. The ponderomotive potential is $U_p = 2.2 \times 10^{-4}$ Ry, thus negligible. The resulting total ionization is $N_{\text{esc}} = 0.038$, which means that the test case stays safely in the perturbative one-photon regime. The s.p. spectrum of the Na_9^+ cluster groups into two shells of nearly degenerated levels denoted in harmonic oscillator labeling as $1s$ and $1p$ [32]. Figure 2 displays the obtained PES (black line) for this laser pulse. The PES shows the typical pattern of one-photon emission. One can nicely identify the two peaks corresponding to the two shells, $1s$ and $1p$, of occupied s.p. levels (mind that, in 2D, the $1p$ levels are degenerate), shifted by the laser frequency, as expected from Eq. (1).

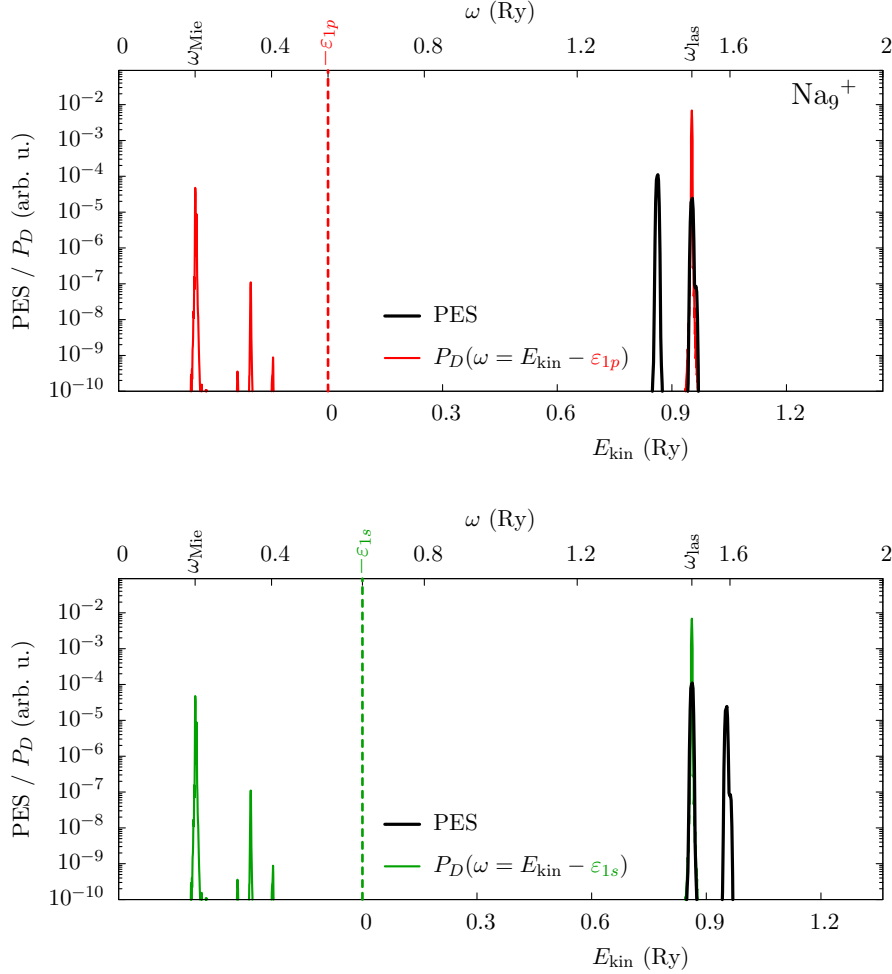


Fig. 2. Excitation of Na_9^+ by a UV laser pulse with frequency $\omega_{\text{las}} = 1.5$ Ry, intensity of 10^{13} W/cm², and total duration 232 fs. PES (black curve, lower x -axis in each panel) is compared with the spectral distribution of dipole power $P_D(\omega)$, one shifted by ε_{1s} (bottom panel) and the other shifted by ε_{1p} (top panel) according to Eq. (1). PES is drawn versus the kinetic energy E_{kin} of the emitted electron and exists, of course, only for positive E_{kin} , while the dipole power P_D shifted by ε_i also extends to negative energies. The vertical dashed line indicates the emission threshold at $E_{\text{kin}} = 0$. PES and P_D are drawn in arbitrary units and are scaled such that they have comparable peak heights.

Figure 2 also shows the dipole power distribution $P_D(\omega)$ computed from the response $D(t)$ to the given laser pulse. The power spectrum is compared with the PES twice, once shifted by the s.p. energy $\varepsilon_{1s} = -0.64$ Ry (bottom panel) and once shifted by $\varepsilon_{1p} = -0.55$ Ry (top panel). These $P_D(\omega = E_{\text{kin}} - \varepsilon_i)$ represent the generalization of Eq. (2) from one dominant laser frequency ω_{las} to a full spectrum ω . Let us now analyze in more detail $P_D(\omega)$ (we remind that the scale for ω appears as the upper horizontal scale in each panel). It shows two prominent peaks: the leading, expected, one at ω_{las} arising from the laser field and a small secondary peak at lower frequency $\omega_{\text{Mie}} = 0.2$ Ry

corresponding to the much celebrated Mie plasmon resonance ω_{Mie} . As it is visible in the right parts of each panel of Figure 2, the laser peak of P_D shifted by the two ε_i perfectly coincides with the two PES peaks. One may be surprised by the appearance of a Mie resonance peak because the mismatch between $\omega_{\text{Mie}} = 0.2$ Ry and $\omega_{\text{las}} = 1.5$ Ry is huge. Remind however that the laser pulse has a finite width. Therefore, even at ω_{Mie} , there remains a faint piece of spectral strength in the laser signal which together with the overwhelming responsivity of the Mie plasmon produces this sidepeak. Although visible, it is naturally suppressed by orders of magnitude and has no impact on the PES here.

Thus far, the picture is straightforward for such a simple laser pulse. The analysis will nevertheless quickly grow in complexity when proceeding to more involved pulses with a richer spectral pattern, because it has to be performed with the two occupied electron shells in the case of Na_9^+ . To simplify the picture at the side of the test system, we will concentrate, from now on, on the simpler case of an helium atom with one single occupied level (with two electrons of opposite spins). It should also be noted that the Helium case is especially interesting in our framework as it involves only one (doubly occupied) wave function. For then the self interaction correction which we use [40] exactly removes the self-interaction error at all orders.

3.2 Dipole boost excitation

We start the studies on the He atom by first considering a simple boost excitation (simulating a collision with a fast charged projectile). Figure 3 shows the emerging PES (black) together with the dipole power spectrum P_D (red). In that case, the simple rule Eq.(1) is by construction not applicable because there is no laser around imprinting its frequency ω_{las} onto the process. On the other hand, and following the analysis of Section 3.1, one can still compare the distribution of PES and the dipole spectrum $P_D(\omega = E_{\text{kin}} - \varepsilon_{1s})$, as is done in Figure 3. The sequence of peaks in PES nicely matches a similar sequence in P_D when shifting the scales by the s.p. energy of the single occupied state $1s$ (which is here identical to the IP). The agreement between both curves is striking, primarily concerning the location of peaks and, to a large extent, even at the side of the relative heights of peaks. This confirms the findings of Figure 2, but now in a case where the simple rule Eq. (1) is by definition meaningless. The generalization of the rule (1) which we read off from Figure 3 is that the whole distribution of PES yield is strongly related to the, properly shifted, dipole power, i.e., $\mathcal{Y}(E_{\text{kin}}) \leftrightarrow P_D(\omega = E_{\text{kin}} - \varepsilon_{1s})$, both to be read as a function of E_{kin} . This is the conjecture which we now want to scrutinize further.

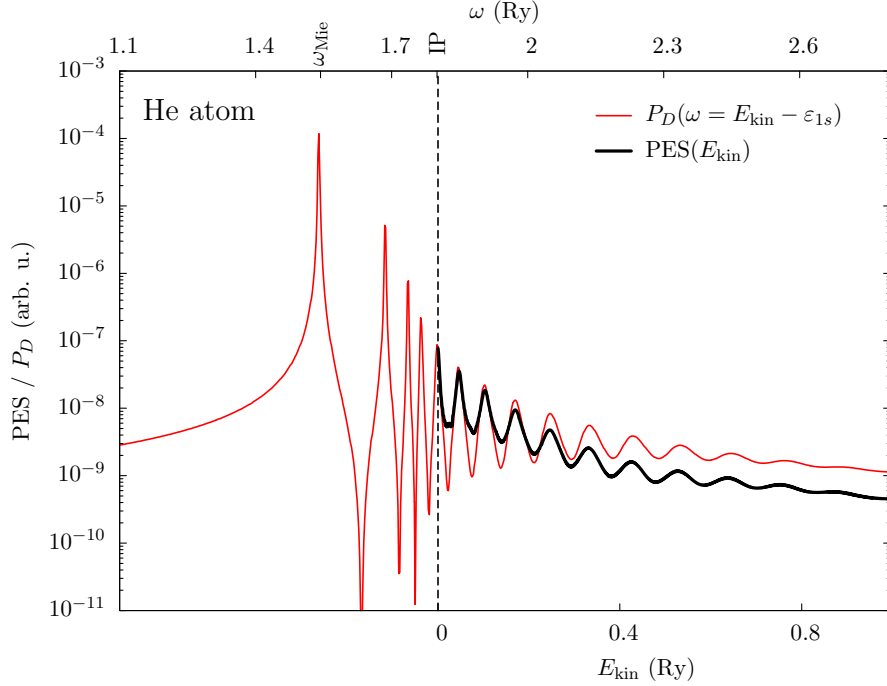


Fig. 3. He atom excited by instantaneous dipole boost of $0.001/a_0$. Photo-Electron Spectra (black line and lower horizontal scale on E_{kin}) and dipole power P_D shifted by the energy of the s.p. level, $\varepsilon_{1s} = 1.8$ Ry, (red line and upper horizontal scale on ω). The key for P_D indicates that it can be read in two ways, either vs. ω (upper x -axis) as usual for a spectrum, or vs. E_{kin} (lower x -axis) for comparison with PES. The vertical solid line denotes the ionization potential (IP).

3.3 An attotrain excitation

The case of a simple boost produces a relatively simple dipole spectrum P_D with only a few dominant peaks and minor ones (which, nevertheless, show up in the PES). It is thus also interesting to see how the above conjecture performs in a complicated case involving several laser frequencies on top of the eigenfrequencies of the system. This situation is illustrated in Figure 4, again in the helium atom. The latter one is irradiated by the attosecond laser train defined in Eqs. (5). It consists out of $N = 7$ individual UV pulses, each one of duration $T = 1$ fs. The time interval between the end of an attopulse and the onset of the next one is 0.33 fs. Therefore, we have $T_{\text{train}} = 1.33$ fs, corresponding to a frequency $\omega_{\text{train}} = 2\pi/(1.33/0.0484) = 0.23$ Ry to the system. The lower panel of Figure 4 shows the result for PES and $P_D(\omega)$. For the sake of completeness, we also show the power spectrum of the electric field $P_{\text{atto}}(\omega)$ defined as $P_{\text{atto}}(\omega) = |\tilde{E}_{\text{atto}}(\omega)|^2$ where $\tilde{E}_{\text{atto}}(\omega)$ is the Fourier transform of the laser field of the attopulse train $E_{\text{atto}}(t)$. The dipole power spectrum P_D now takes a seemingly complicated “comb” structure which, however, can be understood in simple terms. One identifies a wide peak located around the attosecond frequency $\omega_{\text{atto}} = 1.69$ Ry (see upper horizontal scale;

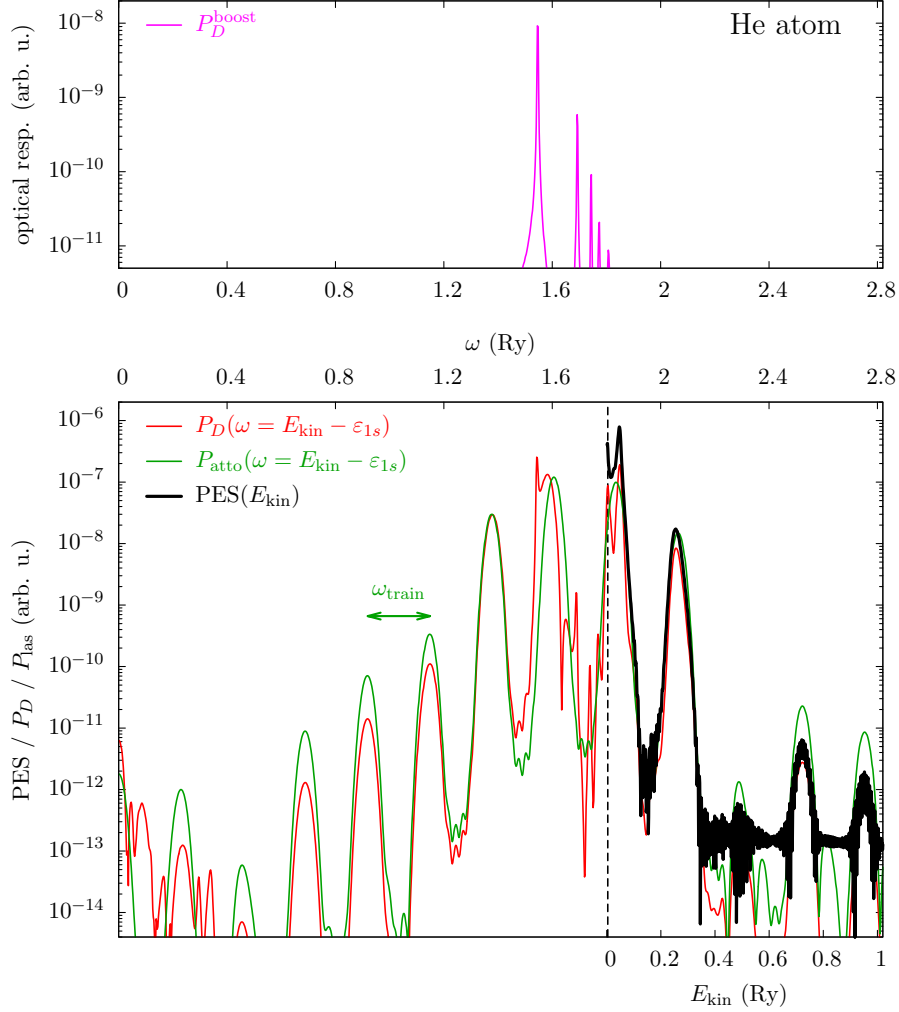


Fig. 4. Lower: PES (black) and dipole power P_D (red) for a He atom excited by the attosecond pulse train (APT) as given in Eq. (5), see text for details. The green line shows the power spectrum P_{atto} of the laser field delivered by the attopulse train. The vertical dashed line indicated the ionization threshold. Upper: The optical response P_D^{boost} of the He atom.

mind that there is a Gaussian envelop to the attotrain, see Eq. (5a), so that the maximum of P_{atto} is not exactly at ω_{atto}). It has a large width of about 0.3 Ry related to the short duration of only 1 fs. Because the signal is repeated in time (attotrain), this broad structure is overlaid by more intense and sharper structures precisely separated from each other by ω_{train} , corresponding to the repetition rate of the pulses. As the IP of the He atom is 1.80 Ry, only the high energy wing of these structures shows up in the PES. And the agreement between $P_D(\omega)$ and PES is striking for this part of the spectrum : Again, both the position and relative heights of major PES peaks just map the dipole spectrum (mind the logarithmic ordinate scale and the orders of magnitude suppression of higher energy PES peaks).

It is also interesting to note that the dipole power $P_D(\omega)$ (red curve) does not follow exactly the power of the external field $P_{\text{atto}}(\omega)$ (green curve). To understand these discrepancies, the upper panel shows the pure optical response $P_D^{\text{boost}}(\omega)$ obtained from a pure dipole boost, as that shown in Figure 3. This reflects the dipole eigenmodes of the system. There are marked differences between P_{atto} and P_D exactly at the places where we observe strong peaks in P_D^{boost} . This indicates that the spectrum of the dipole response $P_D(\omega)$ combines structures from both the laser field (i.e. from P_{atto}) and the strongest eigenmodes of He in P_D^{boost} . This by itself is not surprising. What is more interesting is the fact that the PES precisely matches the combination of both spectra as given in P_D , down to details of peak splittings. This is especially clear for very low energy PES peaks in which secondary peaks of $P_D^{\text{boost}}(\omega)$ are still visible. This example of an attotrain thus confirms our previous findings, namely that $P_D(\omega = E_{\text{kin}} - \varepsilon_{1s})$ is strongly related to the PES. The simple estimate remains robust even for an involved pulse plus admixtures of system frequencies in P_D .

4 Towards a general and robust interpretation of PES

4.1 *The surprising case of an attotrain combined to an IR laser*

There remains an interesting case to be explored in connection to attosecond trains. In most experiments [26,43,44,45], an IR pulse is used to generate high harmonics which then serve to produce the coherent attotrain. Therefore, the attotrain is shot on top of the IR pulse, the latter one provoking slow and gentle dipole oscillations of the electron cloud. We use here an IR pulse with the profile Eq.(4a) and the parameters $\omega_{\text{las}} = \omega_{\text{IR}} = 0.115$ Ry, an overall pulse length $T = T_{\text{IR}} = 105$ fs, and a field strength of $E_0 = 0.0034$ Ry/ a_0 (that is, an intensity $I_{\text{IR}} = 10^{11}$ W/cm²). The IR pulse alone does not ionize the ground state of He atom, while the UV attotrain on top of the IR pulse leads to a measurable ionization. The result of such a setup is shown in Figure 5, again comparing the PES and the dipole power P_D . At variance with all previous cases, the two spectra do not coincide anymore. Only half of the peaks of the PES can be found in the dipole spectrum P_D . Another sizeable ingredient is thus clearly missing in this case.

4.2 *Beyond dipole response*

Let us remind that P_D is the Fourier transform of the time evolution of the electronic dipole. A laser pulse, being $\propto \hat{D}$, therefore excites predominantly

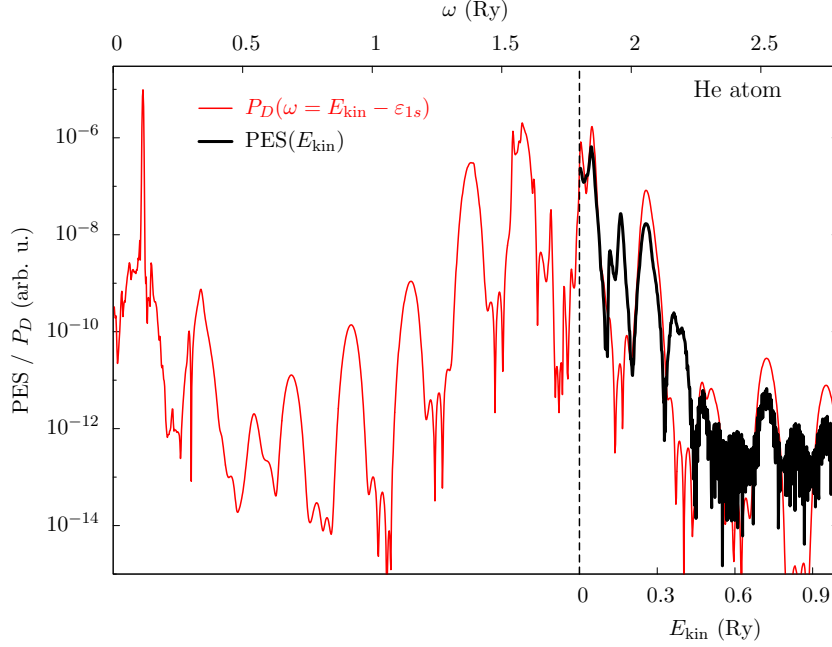


Fig. 5. PES (black) and dipole power P_D (red) for a He atom excited by a combination of an attotrain (5) (as used in Figure 4) with an IR pulse, see text for details. The vertical solid line indicates the ionization threshold.

the dipole. However, strong pulses can also induce higher order deformation of the electron cloud. For example, a dipole shift of the many-electron wave function is realized by the operation

$$|\Phi_d\rangle = e^{-id\hat{P}}|\Phi_0\rangle \approx \left(1 - id\hat{P} - \frac{1}{2}d^2\hat{P}^2\right)|\Phi_0\rangle \quad (7)$$

where \hat{P} is the operator of total electron momentum and d the size of the shift. Only the term $\propto \hat{P}^1$ is usually accounted for in case of very weak fields as they are used typically for nanosecond pulses. Such extremely weak pulses can excite only modes with odd parity. Pulses in the femtosecond regime, as used here, deal with stronger (although still moderate) intensities. And this brings also the term $\propto \hat{P}^2$ into play which, in turn, triggers modes with even parity. The leading even parity modes are found in the quadrupole (deformation) and monopole (stretching/compression) channels. The corresponding observables are :

$$Q = \int d\mathbf{r} \hat{Q} \varrho = \int d\mathbf{r} (3z^2 - x^2 - y^2) \varrho(\mathbf{r}) \quad (8)$$

$$M = \int d\mathbf{r} \hat{M} \varrho(\mathbf{r}) = \int d\mathbf{r} r^2 \varrho(\mathbf{r}) \quad (9)$$

where $\varrho(\mathbf{r})$ is the local electron density. Both can be constructed by angular-momentum reduction of a tensor built from the square of a dipole $\mathbf{r} \otimes \mathbf{r}$ [56]. Let us consider for the moment the quadrupole case. Considering the deformed

state defined in Eq.(7), we find

$$\langle \Phi_d | \hat{Q} | \Phi_d \rangle = \underbrace{\langle \Phi_0 | \hat{Q} | \Phi_0 \rangle}_{=0} - id \underbrace{\langle \Phi_0 | [\hat{Q}, \hat{P}] | \Phi_0 \rangle}_{=0} + \frac{d^2}{2} \underbrace{\langle \Phi_0 | [\hat{P}, [\hat{Q}, \hat{P}]] | \Phi_0 \rangle}_{\neq 0} \quad (10)$$

which shows that the second order term can produce, indeed, a finite quadrupole momentum. Whereas the observable P_D can measure only the odd-parity modes, the PES measuring operator is an outgoing wave, approximately $\varphi_{\mathbf{k}} \propto e^{i\mathbf{k}\cdot\mathbf{r}}$, which contains odd and even parities. Thus the PES is, in principle, able to record also even-parity modes. The idea is now that the PES peaks which are missing in P_D correspond to even-parity excitations and thus should show up in the power spectrum of the quadrupole P_Q and/or monopole P_M .

4.3 A pure quadrupole excitation as a proof of principle

Before attempting to analyze the spectrum of Figure 5 with even-parity strengths, one should check whether such a picture makes sense in a “cleaner” case avoiding that the quadrupole contribution has to be figured out from a mix with a dominating dipole. It would thus be interesting to consider a pure quadrupole case excluding any dipole. Although it is not clear how to excite a pure quadrupole in practice, it provides an interesting Gedanken experiment worth being explored. We thus consider an instantaneous quadrupole boost to the electron cloud of the He atom, as

$$\varphi_i(\mathbf{r}) \longrightarrow e^{i\lambda\hat{Q}}\varphi_i(\mathbf{r}) \quad (11)$$

where λ provides the amplitude of the boost. The He ground state has even parity and so does the excitation. Thus the dipole moment remains zero (within the numerical accuracy) all over the time evolution and no dipole eigenfrequency is excited in the process. Note that the quadrupole boost mostly leads to quadrupole oscillations, but the pattern are accompanied by small monopole oscillations which, however, are marginal for the present case.

The PES associated to such a quadrupole boost in a He atom is shown in Figure 6. We also plot on the same figure the quadrupole power P_Q which exhibits the actually excited eigenmodes of the system. The coincidence between PES and P_Q is again remarkable, both in peak positions and relative amplitudes. This result tells us that the PES displays the actually excited eigenfrequencies of the system, whatever way the system is excited. In the usual case of dipole excitations, the dipole response is (not surpassingly) exemplified. In a pure quadrupole (no dipole) excitation, the system mostly responds in the quadrupole channel and if one performs a monopole excitation, the system dominantly responds in the monopole channel (not shown here). The actual

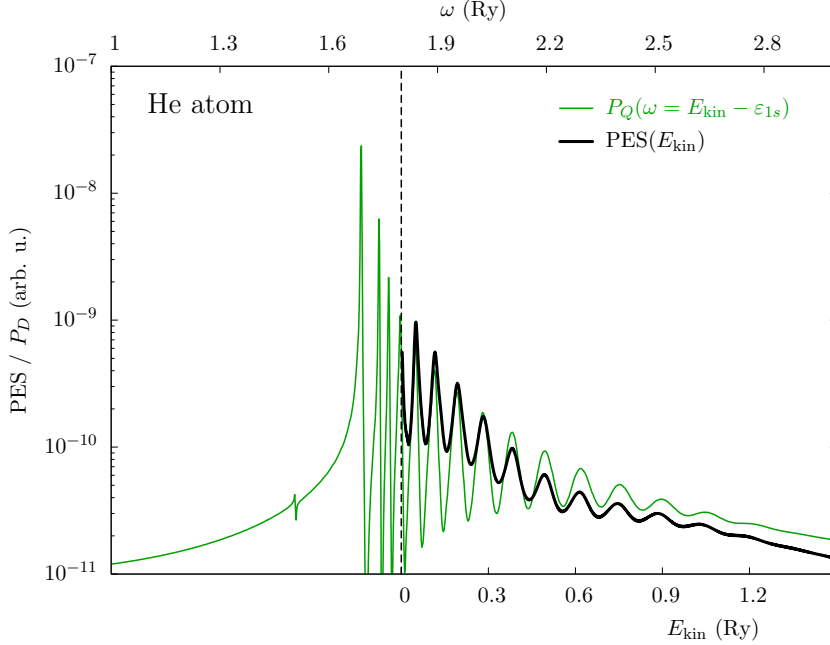


Fig. 6. PES and quadrupole power spectrum P_Q for excitation of the He atom by a quadrupole boost, see Eq. (11), of amplitude of $0.001/a_0^2$.

share of each mode in the response strongly depends on the excitation but as well on the system. As a consequence, one can expect that, for a general excitation, all channels may be excited (though with different strengths) and therefore, one should consider all eigenfrequencies on the same footing. In simple cases, one multipole is dominant so that the other ones do not show up, but this holds not true in general.

4.4 Back to the combined IR + attotrain case

To validate the concept for a more involved case, we come back to the He atom excited by an IR+APT where the dipole response alone could not explain the PES, see Figure 5. We now add the quadrupole spectrum P_Q to the analysis (the monopole spectrum P_M being two orders of magnitude suppressed compared with P_Q , it is not considered here). The result is shown in Figure 7. First note that both P_D and P_Q take similar values after the *same* rescaling to make them match with the PES scale. This is a clear indication that, in this case, both dipole and quadrupole channel do respond with comparable amplitudes. When piling up both P_D and P_Q , one finds a perfect reproduction of the PES, the quadrupole spectrum P_Q precisely bringing the peaks missed by the dipole spectrum. Again the two spectra reproduce both positions and, to a large extent, relative amplitudes, of the PES peaks.

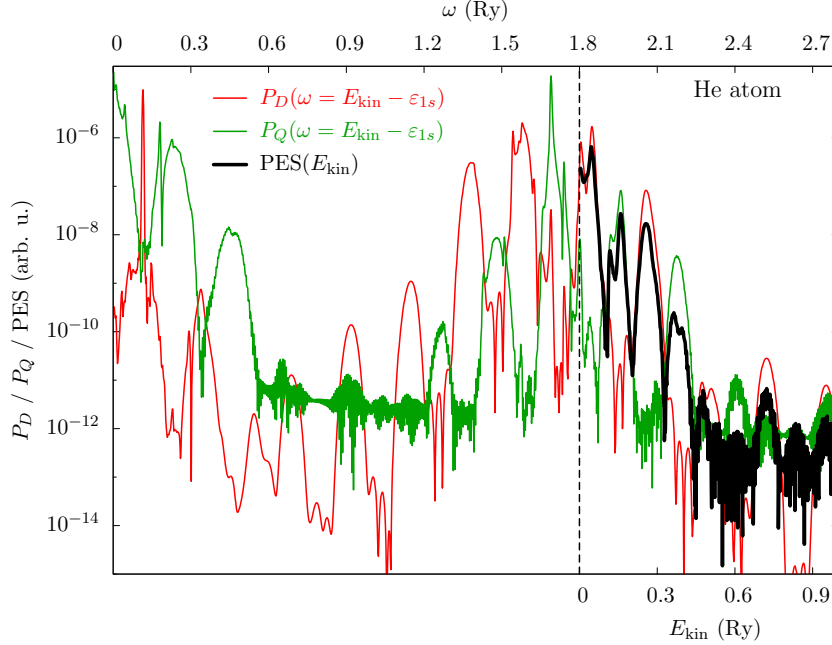


Fig. 7. The same as Fig. 5, but including quadrupole power spectra P_Q . The P_D and P_Q are scaled with the same factor to match the height of the PES peaks.

4.5 The Multi-Photon Ionization regime revisited

Another typical scenario in laser driven dynamics is multi-photon ionization (MPI). We investigate this regime here using a simple laser pulse Eq. (4a) with frequency of $\omega_{\text{las}} = 0.5$ Ry, intensity $I = 10^{11}$ W/cm², and duration $T_{\text{pulse}} = 105$ fs. The frequency, although in the UV regime, is far below the IP of 1.8 Ry. It requires at least four photons to lift an electron into the continuum. This represents a typical MPI case. The result is shown in Figure 8. It is obvious that the dipole power P_D alone cannot explain the whole PES. Remind that a sufficient pulse intensity is required in MPI to allow for multi-photon processes which, in turn, makes co-excitation of even parity modes very likely. The quadrupole power P_Q is sizable, but P_D and P_Q together cannot explain all pattern of the PES in this case. Mind that they both have been scaled the same amount for comparison with the PES, but their relative values have not been touched (the same holds for the monopole below). In fact, P_Q is of minor importance here. There is a sequence of PES peaks at low E_{kin} which stems clearly from the monopole modes seen in P_M . Thus monopole and quadrupole which stay formally at the same level of importance should always be included together in the analysis. It is concluded that the pattern of PES can be reproduced by a proper combination of monopole, dipole, and quadrupole strength distributions.

To conclude this discussion of the MPI regime let us mention the associated regime of above threshold ionization (ATI) induced by high infrared intensities

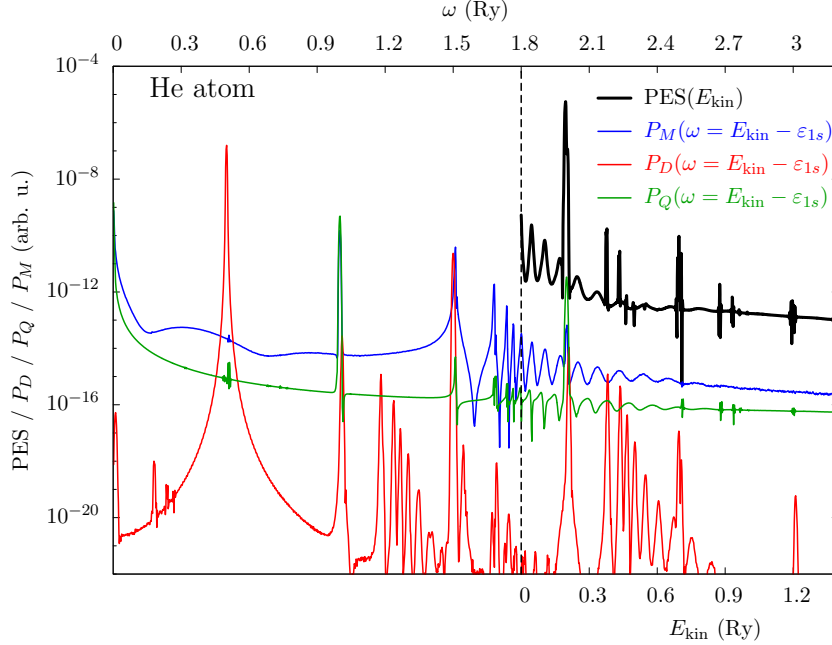


Fig. 8. PES (black), powers spectra of dipole P_D (red), quadrupole P_Q (green), and monopole P_M (blue) for a He atom excited by a UV pulse, see Eq. (4), with a frequency of $\omega_{\text{las}} = 0.5$ Ry, intensity 10^{11} W/cm 2 , and duration $T = 105$ fs.

with $I > 10^{13}$ W/cm 2 [10,42,57,58]. In this case, the ponderomotive energy U_p induces an energetic shift which can become comparable to the laser frequency : for $\omega_{\text{IR}} = 0.11$ Ry, we have $U_p = 0.057$ Ry, which is not negligible anymore. For the sake of simplicity we avoided, in all the above discussions, to consider cases where the ponderomotive shift was important. But in the ATI regime we have to account for this effect. This practically does not change our analysis but for the fact that the multipole spectral distributions have to be shifted by $\varepsilon + U_p$ instead of ε only. But once this precaution has been taken we find that the present spectral analysis of the ATI PES perfectly holds, which perfectly supports our above conclusions.

5 Conclusions and perspectives

We have discussed in this paper the relations between a photo-electron spectrum (PES) and spectral strength distributions of the basic multipole operators (dipole, monopole, quadrupole) for irradiated atoms or clusters. In this investigation, we used a He atom as a test case to have a simple single particle (s.p.) spectrum at the side of the system. For the laser pulses, on the other hand, we consider a variety of scenarios from a simple boost over a one-frequency pulse to complicated mix of IR and atto-second pulses.

Traditionally, there is a simple rule of thumb which relates the position of peaks in the PES to the energies of the occupied s.p. states plus an appropriate multiple of the laser frequency. The simple rule (1) relates peak positions with s.p. energies, or in other words, the consequent estimate of the PES yield, see Eq. (2), relates peaks with peaks. This rule cannot be applied to more complex light pulses which embrace a couple of different frequencies as, e.g., in case of fast collisions with a charge ion or of the mixed pulses typically used in attosecond physics. A natural generalization of it is to model the spectral distribution of PES by the spectral distribution of dipole power $P_D(\omega)$ augmented with s.p. energies. This approach is indeed able to provide a correct picture of PES in some cases. But part of the PES maxima is missing in others. A closer analysis shows that the PES is sensitive to excitations with odd parity as well as those with even parity. However, the dipole spectrum P_D sees only the odd-parity modes. Therefore one must also extend the estimate by strengths of even-parity multipoles. The monopole and quadrupole operator are the most important in that regime. The idea is thus to include, in addition to P_D , the spectral distribution of monopole power P_M and of quadrupole power P_Q into the generalized estimate, which amounts to

$$\mathcal{Y}(E_{\text{kin}}) \leftrightarrow \sum_i \eta_M P_M(E_{\text{kin}} - \varepsilon_i) + \eta_D P_D(E_{\text{kin}} - \varepsilon_i) + \eta_Q P_Q(E_{\text{kin}} - \varepsilon_i) \quad (12)$$

where the sum runs over all occupied s.p. states i , and the η 's factors take care of the relative strength of each eigenmode. Experience gained in the present study suggests that the scaling factors can be taken as being the same for all modes, i.e. $\eta_M = \eta_D = \eta_Q$. This spectrally extended rule (12) has been confirmed for all the types of excitation we have explored, with the contribution of the three terms in the rule varying from case to case. This mapping between response(s) and PES we thus found turns out to be extremely robust.

All in all, the emerging picture remains simple in the sense that the PES still provides a direct printout of the frequencies contained in the response of the system. The simple, traditional, rule (1) is recovered when exciting by a simple mono-frequency pulse sufficiently far from any resonance of the irradiated system. This is the case where we recognize only the laser frequency (and s.p. energies) in the PES. The new rule (12) covers much more general situations. A typical example is attosecond physics where a complex mix of IR pulse with trains of attosecond pulses is often used. There remain widely disputed questions on the mechanisms underlying the response of the system to such complex excitations. A typical observable here is the total ionisation which is found to oscillate with the delay between IR pulse and attotrain [26,27,59]. Our preliminary computations show that these modulations are (not surprisingly) directly reflected in the PES. The robust link we have established with multipole response thus implies a relation between ionisation pattern and multipole response. This is certainly an interesting connection worth being investigated. Work along that line is in progress.

Acknowledgments

We thank P. Salières and R. Taïeb for useful discussions. C.-Z.G. is grateful to the financial support from China Scholarship Council (CSC) (No. [2013]3009). We thank Institut Universitaire de France, European ITN network CORINF and French ANR contract MUSES for support during the realization of this work. It was also granted access to the HPC resources of CalMiP (Calcul en Midi-Pyrénées) under the allocation P1238, and of RRZE (Regionales Rechenzentrum Erlangen).

References

- [1] Turner D W and Jobory M I A 1962 J. Chem. Phys. **37** 3007
- [2] Turner D 1970 Molecular Photoelectron Spectroscopy (New York: Wiley)
- [3] Mainfray G and Manus G 1991 Reports on progress in physics **54** 1333
- [4] Tjeng L H, Vos A R and Sawatzky G A 1990 Surf. Sci. **235** 269
- [5] Hoffmann M A, Wrigge G, v Issendorff B, Muller J, Gantefor G and Haberland H 2001 Eur. Phys. J. D **16** 9
- [6] Liu H and Hamers R J 1998 Surface Science **416** 354
- [7] McHugh K M, Eaton J G, Lee G H, Sarkas H W, Kidder L H, Snodgrass J T, Manaa M R and Bowen K H 1989 J. Chem. Phys. **91** 3792
- [8] Rabalais J 1977 Principles of Ultraviolet Photoelectron Spectroscopy (New York: Wiley)
- [9] Faisal F H M 1987 Theory of Multiphoton Processes (New York: Plenum Press)
- [10] Fennel T, Meiwes-Broer K H, Tiggesbäumker J, Dinh P M, Reinhard P G and Suraud E 2010 Rev. Mod. Phys. **82** 1793
- [11] Agostini P, Fabre F, Mainfray G, Petite G and Rahman N K 1979 Phys. Rev. Lett. **42**(17) 1127–1130
- [12] Eberly J H, Javanainen J and Rzażewski K 1991 Physics reports **204** 331–383
- [13] DeWitt M J and Levis R J 1998 Phys. Rev. Lett. **81**(23) 5101–5104
- [14] Campbell E, Hoffmann K, Rottke H and Hertel I 2001 Journal of Chemical Physics **114** 1716–1719

- [15] Hatamoto T, Okunishi M, Lischke T, Prümper G, Shimada K, Mathur D and Ueda K 2007 Chemical physics letters **439** 296–300
- [16] Keldysh L V 1965 Sov. Phys. JETP **20** 1307
- [17] Keller U 2003 Nature **424** 831
- [18] Rullière C (ed) 2005 Femtosecond Laser Pulses: Principles and Experiments, 2nd ed., Advanced Texts in Physics (New-York: Springer)
- [19] Paschotta R 2008 Encyclopedia of Laser Physics and Technology, volumes 1 and 2 (Berlin: Wiley-VCH)
- [20] Zewail A H 1994 Femtochemistry, Vol. I & II (Singapore: World Scientific)
- [21] Seifert G, Kaempfe M, Berg K J and Graener H 2000 Appl. Phys. B **71** 795
- [22] Andrae K, Reinhard P G and Suraud E 2002 J. Phys. B **35** 1
- [23] Paul P M, Toma E, Breger P, Mullot G, Augé F, Balcou P, Muller H and Agostini P 2001 Science **292** 1689–1692
- [24] Krausz F and Ivanov M 2009 Rev. Mod. Phys. **81**(1) 163–234
- [25] Corkum P and Krausz F 2007 Nature Physics **3** 381–387
- [26] Johnsson P, López-Martens R, Kazamias S, Mauritsson J, Valentin C, Remetter T, Varjú K, Gaarde M B, Mairesse Y, Wabnitz H, Salières P, Balcou P, Schafer K J and L’Huillier A 2005 Phys. Rev. Lett. **95**(1) 013001
- [27] Neidel C, Klei J, Yang C H, Rouzée A, Vrakking M J J, Klünder K, Miranda M, Arnold C L, Fordell T, L’Huillier A, Gisselbrecht M, Johnsson P, Dinh M P, Suraud E, Reinhard P G, Despré V, Marques M A L and Lépine F 2013 Phys. Rev. Lett. **111**(3) 033001
- [28] Kelkar A, Kadhane U, Misra D, Gulyas L and Tribedi L 2010 Phys. Rev. A **82**(4) 043201
- [29] Nandi S, Biswas S, Khan A, Monti J, Tachino C, Rivarola R, Misra D and Tribedi L 2013 Phys. Rev. A **87**(5) 052710
- [30] Dinh P M, Reinhard P G, Suraud E and Wopperer P 2015 Eur. Phys. J. D **69** 48
- [31] de Heer W A 1993 Rev. Mod. Phys. **65** 611
- [32] Brack M 1993 Rev. Mod. Phys. **65** 677
- [33] Hertel I V and Radloff W 2006 Rep. Prog. Phys. **69** 1897
- [34] Pohl A, Reinhard P G and Suraud E 2001 J. Phys. B **34** 4969
- [35] Kohn W and Sham L J 1965 Phys. Rev. **140** 1133

- [36] Gross E K U and Kohn W 1990 Adv. Quant. Chem. **21** 255
- [37] Kümmel S, Brack M and Reinhard P G 1998 Phys. Rev. B **58** 1774
- [38] Goedecker S, Teter M and Hutter J 1996 Phys. Rev. B **54** 1703
- [39] Perdew J P and Wang Y 1992 Phys. Rev. B **45** 13244
- [40] Legrand C, Suraud E and Reinhard P G 2002 J. Phys. B **35** 1115
- [41] Kluepfel P, Dinh P M, Reinhard P G and Suraud E 2013 Phys. Rev. A **88** 052501
- [42] Wopperer P, Dinh P M, Reinhard P G and Suraud E 2015 Phys. Rep. **562** 1
- [43] Johnsson P, Mauritsson J, Remetter T, L’Huillier A and Schafer K J 2007 Phys. Rev. Lett. **99**(23) 233001
- [44] Holler M, Schapper F, Gallmann L and Keller U 2011 Phys. Rev. Lett. **106** 123601
- [45] Klünder K, Dahlström J M, Gisselbrecht M, Fordell T, Swoboda M, Guénot D, Johnsson P, Caillat J, Mauritsson J, Maquet A, Taïeb R and L’Huillier A 2011 Phys. Rev. Lett. **106** 143002
- [46] Calvayrac F, Reinhard P G, Suraud E and Ullrich C A 2000 Phys. Rep. **337** 493
- [47] Reinhard P G and Suraud E 2003 Introduction to Cluster Dynamics (New York: Wiley)
- [48] Reinhard P G, Stevenson P D, Almedhed D, Maruhn J A and Strayer M R 2006 Phys. Rev. E **73** 036709
- [49] Calvayrac F, Reinhard P G and Suraud E 1995 Phys. Rev. B **52** R17056
- [50] Calvayrac F, Reinhard P G and Suraud E 1997 Ann. Phys. (NY) **255** 125
- [51] Pohl A, Reinhard P G and Suraud E 2004 J. Phys. B **37** 3301
- [52] Bär M, Dinh P M, Moskaleva L V, Reinhard P G, Rösch N and Suraud E 2010 Phys. Stat. Sol. B **247** 989
- [53] De Giovannini U, Varsano D, Marques M A L, Appel H, Gross E K U and Rubio A 2012 Phys. Rev. A **85**(6) 062515
- [54] Dinh P M, Romaniello P, Reinhard P G and Suraud E 2013 Phys. Rev. A **87** 032514
- [55] Wopperer P, Reinhard P G and Suraud E 2013 Ann. Phys. (Berlin) **525** 309–321
- [56] Edmonds A R 1957 Angular Momentum in Quantum Mechanics (Princeton: Princeton University Press)
- [57] Campbell E E B, Hansen K, Hoffmann K, Korn G, Tchapyguine M, Wittmann M and Hertel I V 2000 Phys. Rev. Lett. **84** 2128

- [58] Huismans Y, Cormier E, Cauchy C, Hervieux P A, Gademann G, Gijbetsen A, Ghafur O, Johnsson P, Logman P, Barillot T, Bordas C, Lépine F and Vrakking M J J 2013 Phys. Rev. A **88**(1) 013201
- [59] Dahlström J, LHuillier A and Maquet A 2012 Journal of Physics B: Atomic, Molecular and Optical Physics **45** 183001